Study of the dielectric, optical and microstructure properties of CaCu$_3$Ti$_4$O$_{12}$–PbZr$_{0.48}$Ti$_{0.52}$O$_3$ ceramic system with different compositions

Nasr Hadi [1],*, Abdi Farid [1], Taj-Edine Lamcharfi [1], Abdesselam Belaaraj[2], Said Kassou [2] and Fatimazahra Ahjyaje [1]

[1] Laboratory of Signals, Systems and Components, USMBA. FST Fez, B.P. 2202, Morocco

[2] Laboratory Physics of Materials and Systems Modeling CNRST URAC08, Moulay Ismail University, Faculty of Sciences Department of Physics, Morocco

Abstract: In this paper, composite ceramics (1-x)CaCu$_3$Ti$_4$O$_{12}$–(x)PbZr$_{0.48}$Ti$_{0.52}$O$_3$ (with x =0.00, 0.50 and 1.00), denoted CCTO-PZT, were prepared by a three-stages modified method, in order to achieve high dielectric constant and low loss. Structural investigations carried out by X-ray diffraction (XRD), and FT-IR spectroscopy showed the formation of pure cubic and tetragonal phases for x = 0.00 and x=1.00 compositions, respectively. XRD showed the coexistence of both phases in the CCTO-PZT composite. The morphology of the ceramics was examined by scanning electron micrograph (SEM), results reveal a homogeneous microstructure with two types of grains corresponding to PZT (smaller grains) and CCTO (large grains). Dielectric measurements carried out by an impedance analyzer; show that the dielectric constant of the CCTO-PZT composite is higher than the pure samples (CCTO and PZT) one. The temperature dependence of the ac conductivity indicated that the conduction follows the Arrhenius law and the conduction process is due to the single and the doubly ionized. The optical band gap of the PZT is 2.25 eV, and the band gap decreased in the CCTO/PZT composite.

Keywords: CaCu$_3$Ti$_4$O$_{12}$-PbZr$_{0.48}$Ti$_{0.52}$O$_3$; dielectric; optical; electrical; microstructure properties.

Introduction

Lead zirconate titanate PbZr$_{1-x}$Ti$_x$O$_3$ (with x=0 up to 1) (PZT) and Calcium Copper Titanate (CaCu$_3$Ti$_4$O$_{12}$, CCTO) are a perovskite types ABO$_3$ (where A = Pb, B = Ti or Zr for PZT and where A = Ca or Cu and B=Ti for CCTO) have widely used for different applications, due to their excellent dielectric and piezoelectric properties [1-6]. However, it is well known that PZT-based ceramic materials are not environmentally friendly because of the PbO evaporation during sintering. Furthermore, the PbZr$_{1-x}$Ti$_x$O$_3$ (PZT) is a ferroelectric perovskite and has a tetragonal, or/and rhombohedral and orthorhombic phases depending on the value of Zr/Ti ratio. It has two morphotropic phase boundaries (MPB) at 53/47 and 95/5 Zr/Ti ratio[7]. On the other hand, CaCu$_3$Ti$_4$O$_{12}$ (CCTO) ceramic has a high dielectric constant (10^4) independent of temperature (100–400K) and frequency (10^2–10^6 Hz) [6,7], which makes it a promising material for application in microelectronics, but unfortunately, CCTO ceramic exhibits high dielectric loss that limits its practical applications in electronic industries. Based on this, researchers and technologists are intensively developing lead-free and thermally stable high ε$_r$

material as alternatives, which have a constant value over a wide frequency region. Among those efforts, extensive studies of the formation of perovskite oxides of the systems Ca$_{1-x}$M$_x$Ti$_{1-x}$M$_x$O$_3$ (M = Cu, Y, Sr, Ba, Pb, Zr, Co, Al, Fe, Li, Cr) were performed as attempts to improve the properties of ceramic materials [8]. At present, research work has begun on the basis of the idea of integrating ceramic materials, among them; Almeida et al. [9], they studied the properties of the composite (1-x)BaTiO$_3$–xCCTO film (x=0.00,0.50 and 1.00), N. Hadi et al. [10] investigated the dielectric properties of the (1-x)CCTO-xBaTiO$_3$ composites. In an analogous previous work [11], we investigated the properties of the (1-x)CCTO-xPZT composite ceramics with a ratio Zr/Ti = 65/35, beyond the morphotropic phase and for which PZT presents a tetragonal phase. Our results showed that the composite CCTO-PZT with the content near 50% of PZT has the great value of the maximum of the dielectric permittivity. Rajabtabar et al. [12] have investigated the dielectric properties of CaCu$_3$Ti$_4$O$_{12}$/Pb(Zr$_{0.52}$Ti$_{0.48}$)O$_3$, the considered ratio Zr/Ti of PZT corresponds to the morphotropic phase with the coexistence of both rhombohedral and tetragonal phases of PZT, their

results showed that the composite ceramics with the $Pb(Zr_{0.52}Ti_{0.48})O_3$ content of 20% has the highest dielectric constant and the lowest dielectric loss. In the present research, a new CCTO-PZT with a ratio Zr/Ti=48/52 which is close to the morphotropic phase boundary with a single tetragonal phase was synthesized from PZT and CCTO which were prepared by sol-gel and solid state route respectively. We investigate the dielectric, electrical, structural and optical properties of the synthetized samples. Also, the relationships between the microstructure and dielectric properties of the PZT, CCTO and CCTO-PZT ceramics were discussed.

Experimental

The (1-x)CCTO-xPZT (where x = 0.00, 0.50 and 1.00) ceramic composites were synthesized by a modified route via three steps. Firstly, CCTO was synthesized by a solid-state reaction using $CaCO_3$, CuO and TiO_2 were used as raw materials. In this route, stoichiometric ratios of the reagents were mixed in an agate mortar for 1h, after that stirred in the medium of acetone for 3h, then ground again. The mixed powder calcined in air at 1050 ^{0}C for 4h. Secondly, $PbZr_{0.48}Ti_{0.52}O_3$ (PZT) ceramic powder was synthesized by a Sol-Gel process using zirconium acetate, $Zr(CH_3COO)_4$, Lead (II) acetate trihydrate, $Pb(CH_3COO)_2.3H_2O$ and titanium isopropoxide, $Ti(OCH(CH_3)_2)_4$. The metal acetates were dissolved in distilled water to obtain standard aqueous solutions of Pb^{2+} and Zr^{4+} and mixed in separate beakers along with stoichiometric amounts of $Ti(OCH(CH_3)2)_4$.

PZT gel formed. The dry gel was calcined at 700 °C for 4 h in the atmosphere. Finally, the (1-x)CCTO-xPZT prepared of CCTO and PZT were carefully weighed in stoichiometric proportion and mixed thoroughly in an agate mortar for 1h then stirred in acetone for 2h. The powder was then dried at 400 °C for 2h. The dried powder was then pressed into disks of 12mm as diameter and 1mm of thickness under pressure around 430 MPa and using the polyvinyl alcohol (PVA) as a binder. The final sintering of the pellets was done at 1000 ^{o}C for 8h with a heating rate of 3 ^{o}C/min

Results and discussion

X-ray diffraction patterns of the CCTO, PZT and CCTO-PZT ceramic are shown in Figures 1a, 1b, and Figure 2, respectively. The PZT and CCTO ceramics show a single phase, which is highly crystalline in nature where the main peaks of the ceramic powders are comparable to those of the standard ceramic XRD patterns of PZT (JCPDS 33-0784) and CCTO (JCPDS 75-2188), which have been indexed to Im-3 and P4mm space groups with cubic and tetragonal symmetries respectively. For the CCTO-PZT composite, each XRD pattern can be disassembled into two evident sets of well-defined peaks that belong to the PZT and CCTO phases without a secondary one. A similar result has observed in (Nylon11 + µCCTO) composites [13] where both the Nylon11 and µCCTO peaks were observed to be unchanged.
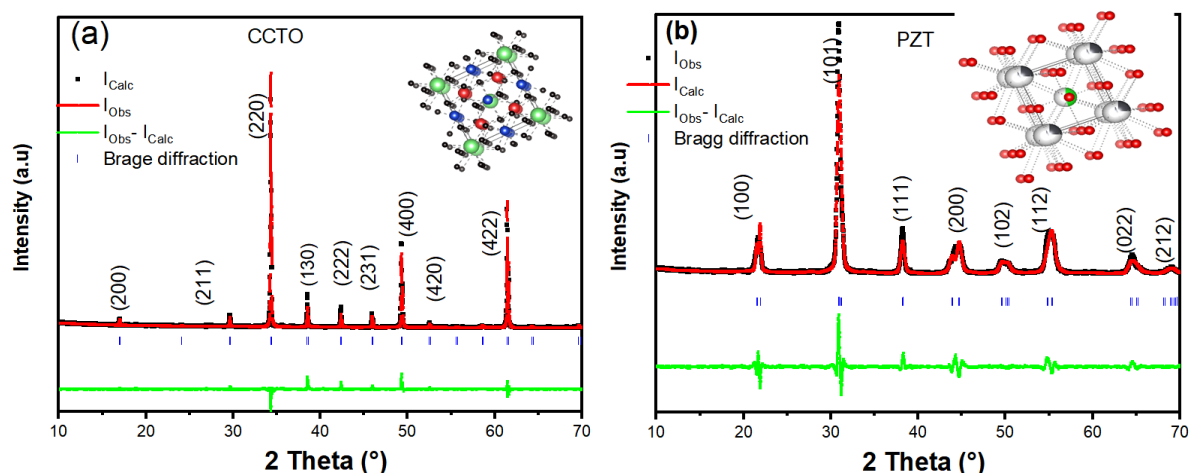

Figure 1. XRD patterns and their Rietveld refinements for a) CCTO and b) PZT (48/52) samples.

The XRD patterns have been analyzed by employing the Rietveld method using Fullprof Software program [14] using the Im-3 and P4mm space groups for CCTO and PZT, respectively. The X-ray diffraction patterns along with Rietveld refined data hare shown in the Figures 1a, 1b and Figure 2. In these figures, the black points represent our experimental results, and the solid line (red) represents Rietveld refined data. The bottom lines

show the difference between the experimental and refined data. The small vertical lines (blue) represent Bragg allowed positions. From Rietveld analysis, the crystalline structure was confirmed, and the unit cell parameters calculated. The lattice constants, we obtain for pure CCTO, and PZT (Table 1) are in good agreement with those reported in literature [15-17]. In the case of the (CCTO -PZT) mixture, Rietveld analysis shows that the crystal structure is a composition of

both CCTO and PZT structures as separate ones, the same phenomenon has been observed for The BaM/CCTO composites which exhibit a single crystalline phase of both BaM and CCTO[18]. However, we remark a slight change in the lattice parameters. The lattice constant decreased in CCTO while it increased in PZT accompanied by a decrease in *c*.

The fitting quality of the experimental results has been assessed by computing the parameters such as the "fit goodness" X^2, R_B (Bragg factor) and R_F (crystallographic factor) [14] obtained from Rietveld refinement. They are given in Table 1 for all the samples.

The Crystallite size (D) of the compounds was determined by the Scherrer's formula [19]. We can notice that the crystallite size of CCTO was found to decrease on adding PZT while the PZT crystallite size increases (Table 1).
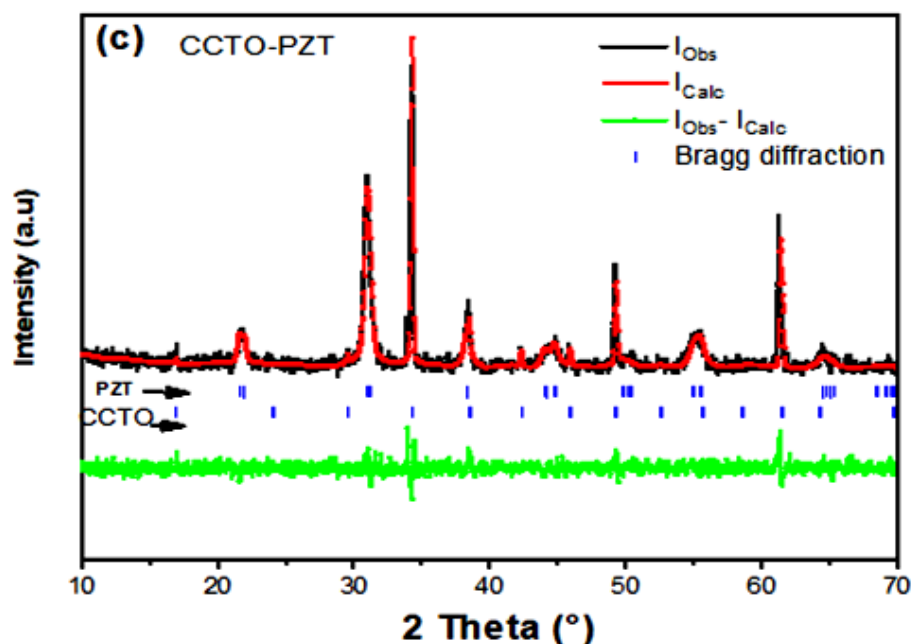

Figure 2. XRD pattern and Rietveld refinement for the CCTO-PZT sample

Table 1. Reliability factors (R_{Bragg}, R_F and X^2), crystalline size (D), lattice parameters and cell volume V for CCTO, PZT and CCTO and PZT in the mixture.

Parameters	CCTO	PZT	CCTO-PZT	
			CCTO	PZT
R_{Bragg}	6.31	6.69	9.01	4.42
R_F	7.98	9.26	7.76	2.79
X^2	2.19	2.93	1.13	1.13
D (Å)	597. 4	126.5	556.2	130.6
a. b and c (Å)	a=b=c=7.3 905	a=b=4.0449 and c=4.11118	a=b =c=7.38876	a=b=4.04603 and c=4.10945
c/a	1	1.06386	1	1.0567
V (Å³)	403.665	67.264	403.381	67.273

The formation of the phases and purity of CCTO and PZT were confirmed from the FT-IR spectrum shown in Figure 3. The IR spectra of the CCTO perovskite in the region of 400–1200 cm^{-1} is dominated by three broad absorptions centred at 566, 516 and 447 cm^{-1} [9,11]. A similar spectrum for the ceramic CCTO we prepared in our study is observed,

with absorptions at 573, 523 and 451 cm^{-1} (Figure 3). These absorptions are related to Ca-O, Cu-O and Ti-O-Ti, respectively.   For the PZT (48/52) perovskite, two mains absorptions were observed at 576 and 400 cm^{-1}, which is consonant for the PZT perovskite [11]. For both the samples, a broad absorption band is observed at 1000 – 600 cm^{-1} that

suggests a structural rearrangement of the BO_6 unit   resulting in perovskite phase formation.
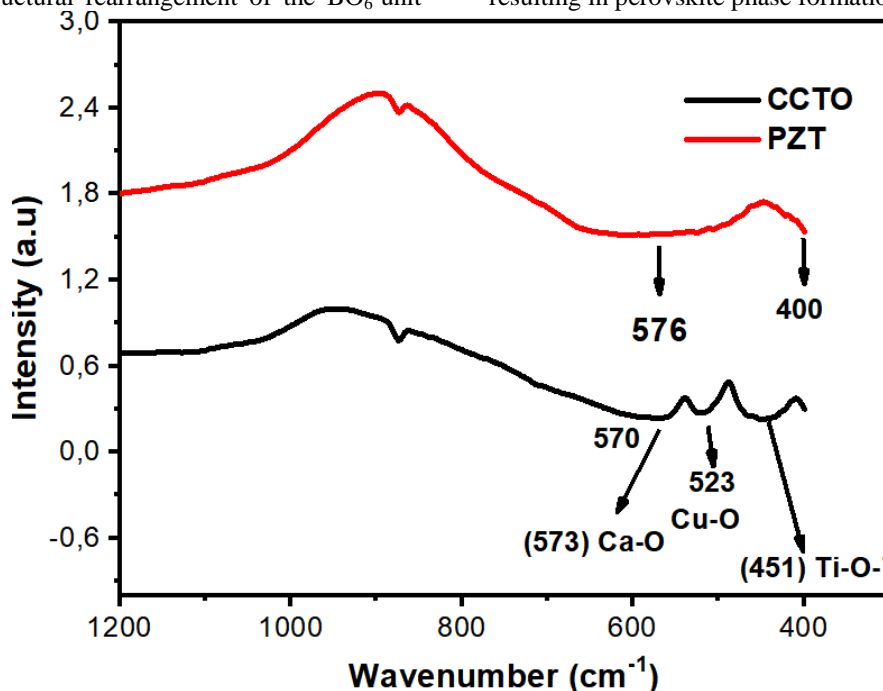

Figure 3. FT-IR spectrum of pure CCTO and PZT.

Figure 4 shows scanning electron microscopy (SEM) images of the PZT, CCTO and CCTO-PZT pellets sintered at 1000 °C for 8 h. The average grain sizes of the CCTO, PZT and CCTO-PZT pellets were found to be 8.75, 6.01 and 1.75 μm, respectively. PZT (48/52) shows a dense microstructure and the presence of many clusters. The CCTO ceramics exhibited a completely homogeneous morphology with abnormally large grains with a small grain segregated at the grain boundaries. The grains of CCTO have smooth surfaces associated with a spherical appearance, while the morphology of the CCTO-PZT ceramic shows the unique features with a large conglomerate formed by a cluster of small granules with the presence of large pores between these conglomerates.
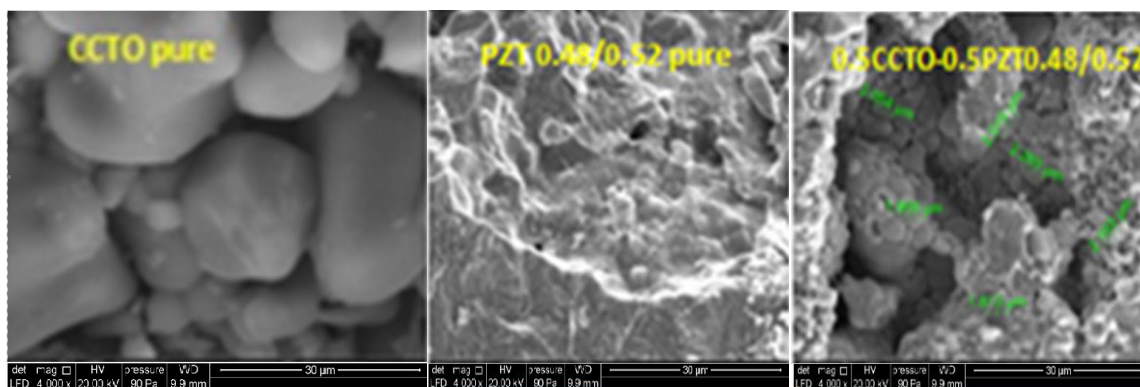

Figure 4. SEM micrographs for CCTO (ref 11), PZT and (1-x)CCTO-xPZT for $x = 0.00$, 0.50 and 1.00

Since the modification of the grain size of the ceramics affects the dielectric responses, we investigate the dielectric properties of our synthetized samples. The temperature dependence of the dielectric properties of the CCTO, PZT and CCTO-PZT ceramics sintered at 1000 °C for 8 h at the frequency of 10 kHz is shown in Figure 5a. We can see that ε'_r increases up to maximum values 27620 at 400 ^{0}C for PZT and 18205 for CCTO-PZT at 363^{0}C, and then ε'_r decreased with increasing temperature. The temperature at which the transitions occur is termed the Curie temperature, (T_c), where PZT undergoes a transition from a ferroelectric to a paraelectric. The figure shows a shift of Tc to low temperatures for CCTO-PZT composite, while for CCTO sample an abroad dielectric peak appeared between 150 and 400 °C. Figure 5b shows the frequency variation of the dielectric constant (10^2 up to 2.10^6 Hz) at room temperature for all composites. The values of ε'_r for the CCTO, PZT and CCTO-PZT samples at 1 kHz are found 1662, 957and 4923, respectively. It can be

seen that the value of the dielectric constant (ε'_r) for the CCTO-PZT ceramics is higher than the values of the CCTO and PZT ceramics. The ε'_r decreased with
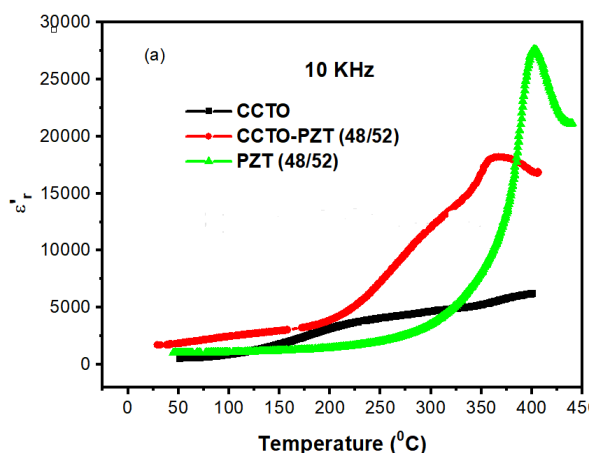
increasing frequency in CCTO and CCTO-PZT samples, but it remains independent of frequency in pure PZT.
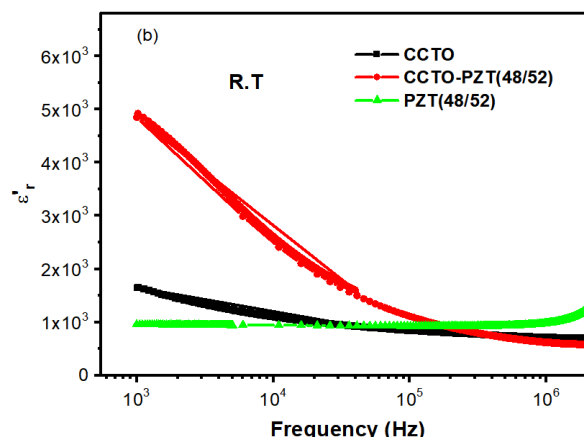

Figure 5. Real part of the relative dielectric constant of CCTO, PZT and CCTO-PZT as a function of (a) temperature at 10 kHz (b) frequency at R.T

Many researchers interpreted the relaxation behavior in the CCTO ceramic samples through the complex impedance spectrum by three semicircles in Nyquist plot or three peaks in electric modulus plot (M" versus frequency plot), and modeled the dielectric response into an equivalent circuit which consists of three parallel RC elements connected in series [16]. For the same purpose, in our study, the frequency ranged from 100 Hz to 2 MHz. The impedance spectrum study of all samples with increasing temperature showed that at lower temperatures, only one semicircular arc (data not shown). This suggests the presence of grain bulk properties (capacitance and resistance) of the materials. However, at higher temperatures, the semicircle arc is distorted, and another arc appears,

and the spectrum includes two semicircular arcs with their centers lying out of the real axis for all samples (Figure 6). This means that the relaxation process becomes non-Debye. This behavior can originate from several factors such as grain boundary, grain size distribution or orientation, defects distribution, and so on. Thus the presence of two semicircle arcs indicates the presence of both bulk and boundary contributions and the electrode interface effects [20] to the electrical properties of the samples [16]. The equivalent resistance is connected to the diameter of the semicircle arcs, so we can observe that in the studied frequency range the PZT resistance was larger that CCTO and CCTO-PZT resistance as is shown in the Figure 6b.
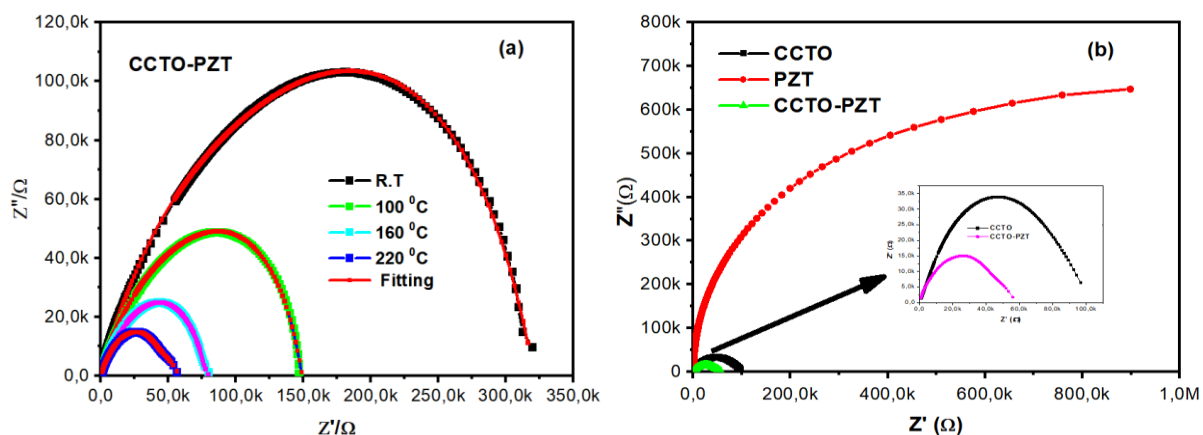

Figure 6. Impedance spectrum of samples for; (a) CCTO-PZT for different temperatures and (b) CCTO, PZT and CCTO-PZT at 220 ^{0}C

According to impedance spectrum data obtained for pure CCTO and PZT samples, each sample can be represented by several elements. For the pure PZT, two parallel elements, R|C and R|CPE connected in series (Figure 7a), are used to fit the impedance data

sample, while three parallel elements represent the pure CCTO sample (Figure 7b) (R|C-R|C-R|CPE). On the other hand, the CCTO-PZT composite is represented by four parallel elements, three of them

R|C and other R|CPE as shown in Figure 7c. These   circuits gave the best fittings.
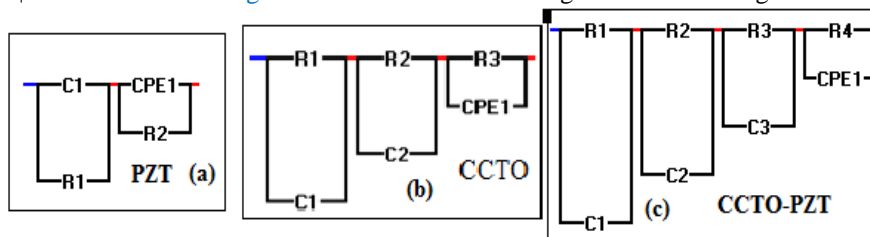

Figure 7. The equivalent electric circuits for the samples: a) PZT, b) CCTO and c) CCTO-PZT.

Figure 8a shows the variation of real (Z') and (Z") part of complexes impedance as a function of frequency (10^2–2.10^6Hz) at different temperatures for CCTO-PZT. We observe that Z' decreases with increasing temperature or frequency and attains a constant value at higher frequencies irrespective of temperatures. This may be due to an increase in the ac conductivity with temperature increasing. The merger of the real part of impedance Z' for all temperatures at the higher frequencies is due to the RC network where the current passes through conducting regions in the material at lower frequencies, but at higher frequencies, the current passes through the insulating (capacitive) regions [9]. The temperature dependence of resistivity showed the typical behavior found for semiconductors. The changes of imaginary part Z'' of impedance for CCTO-PZT ceramic composite are shown in Figure

8b. The typical variation indicates that Z" attains a maximum value at a particular frequency. The maximum value and the frequency position of this maximum depend on temperature. The behavior of Z" shows a considerable decrease in the magnitude with a shift in the peak frequency position towards the higher side when the temperature increases. This feature becomes notable at a higher temperature. The trend of variation of Z" with a shift in the peak frequency suggests the presence of electrical relaxation phenomenon in the material. A relative lowering in the magnitude of Z" accompanied by a shift in the peak frequency position towards the higher side with the rise in temperature originates from the presence of space charges in the material. This result is in good agreement with the observation of complex impedance spectrum results in the literature [6,16].
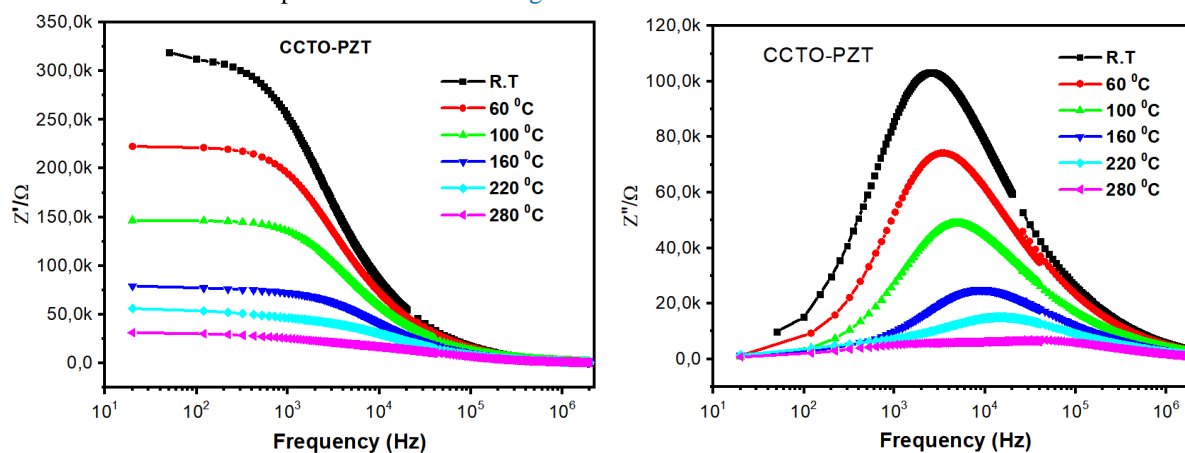

Figure 8. Frequency variations of a) the real part Z´ and b) the imaginary part of CCTO-PZT (48/52) ceramic at different temperatures.

The maximum values Z''_{max} of Z" follow the temperature dependent Arrhenius law, where the frequency position f_{max} associated with Z''_{max} can be expressed as:

$$f_{max} = f_0 exp\left(-\frac{E_a}{K.T}\right)$$

Where E_a is the activation energy in the relaxation process, f_o is the pre-exponential factor, K is the Boltzmann constant and T is the absolute

temperature. Figure 9 shows a plot of log(f_{max}) vs 1000/T for CCTO-PZT composite with the theoretical fit along to the above equation. The slop of the curve gives the value $-\frac{E_a}{2K}$, term enabling us to estimate the activation energy of the samples. The E_a values for all samples are given in Table 2. The activation energy obtained for CCTO-PZT suggests that the conduction process is mainly due a todoubly ionized phenomenon [21].
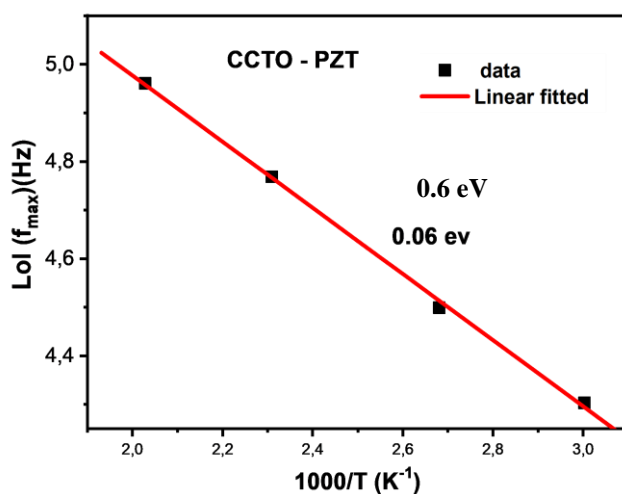
Figure 9. log(fmax) vs.1000/T plot for CCTO-PZT composite

Table 2. Activation energy of CCTO, PZT and CCTO-PZT composite.

Composite	Activation Energy (eV)
CCTO	0.8
CCTO-PZT	0.6
PZT	0.23

In order to understand the mechanism of conduction and relaxation in CCTO, PZT and CCTO-PZT materials, we use the AC conductivity measured as a function of temperature at 10 kHz. As shown in Figure 10, the conductivity of the PZT ceramics remained relatively constant between room temperature up to 50°C. However, as the temperature was further increased, the conductivity increases significantly. The conductivity of the CCTO-PZT pellets is higher than that of the CCTO and PZT ceramics. The high conductivity of the CCTO-PZT ceramic is responsible for the high dielectric constant of this ceramic, which also supports the presence of the IBLC structures [3,17].
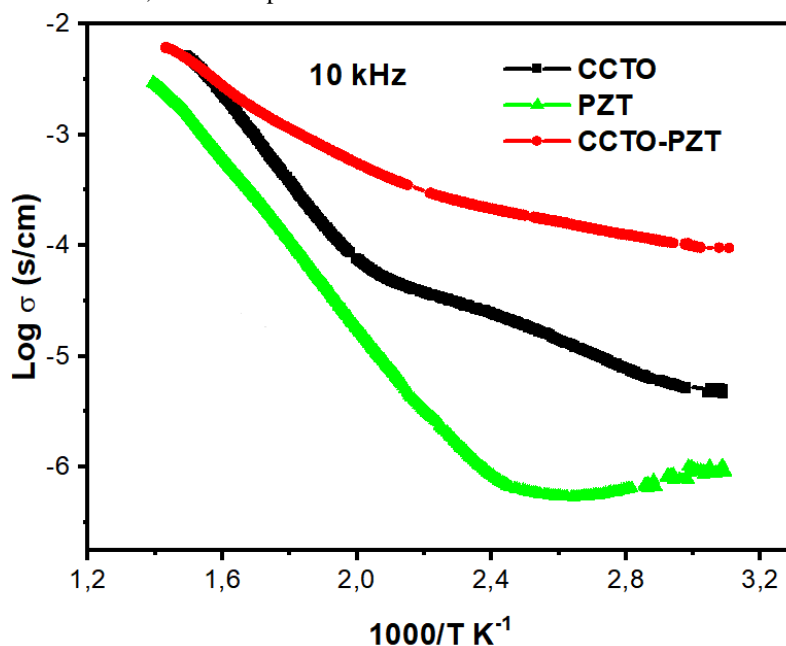

Figure 10. Variation of ac conductivity of CCTO–PZT ceramics with the temperature at 10 kHz.

The UV-visible reflectance spectra of the samples CCTO, PZT and CCTO-PZT, were recorded at room temperature using a Jasco V-570 spectrophotometer, in the wavelength range [200-2000 nm]. A Barium Sulphate plate ($BaSO_4$) is used as the standard (100% reflectance) on which the

crushed sample of the crystal to be analyzed is placed.

The optical transmittance spectrum for the materials CCTO, PZT and CCTO-PZT is shown in Figure 11. The analysis of the spectrums reveals that the pure PZT present a high optical transmittance than the CCTO-PZT and CCTO (Table 3). The high optical transmittance may be due to lesser crystallite size in PZT while the irregular behavior for CCTO and CCTO-PZT could be due to defects mainly originated from CCTO. The scattering is strong, resulting in low transmittance.
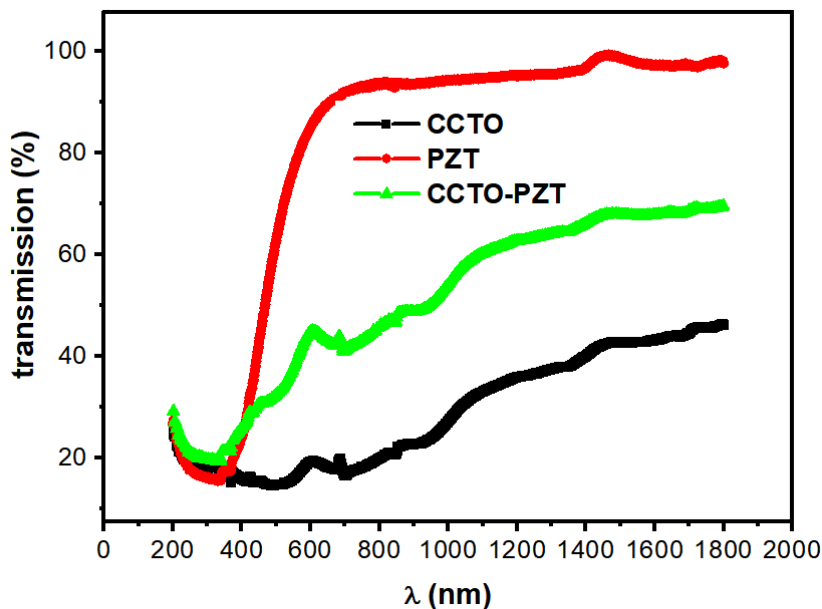

Figure 11. Optical Transmittance spectrum of CCTO, PZT and CCTO-PZT

The dependence of the optical absorption coefficient on the photon energy helps to study the band structure using the following expression.

$$\alpha = \frac{Ln\left(\frac{1}{T}\right)}{d}$$

Where T is the transmittance (%), d is the thickness of the sample (0.76 mm). The optical band gaps energies of the compounds were evaluated using the following expression.

Where A is a constant, E_g is the optical energy band gap, v is the frequency of the incident beam, and h is the Planck's constant. The Eg direct optical band gap energy value is obtained by extrapolating the linear portion of the plot of $(\alpha hv)^2$ versus (hv) to $(\alpha hv)^2 = 0$ as shown in Figure 12. The optical band gap energies (Eg) were found to be 2.25 eV, 3.92 eV, 3.50 eV for CCTO, CCTO-PZT and PZT respectively (Figure 12 and Table 3) the band gap calculated in our study is consistent with the range gap values which mentioned in the literature [22].
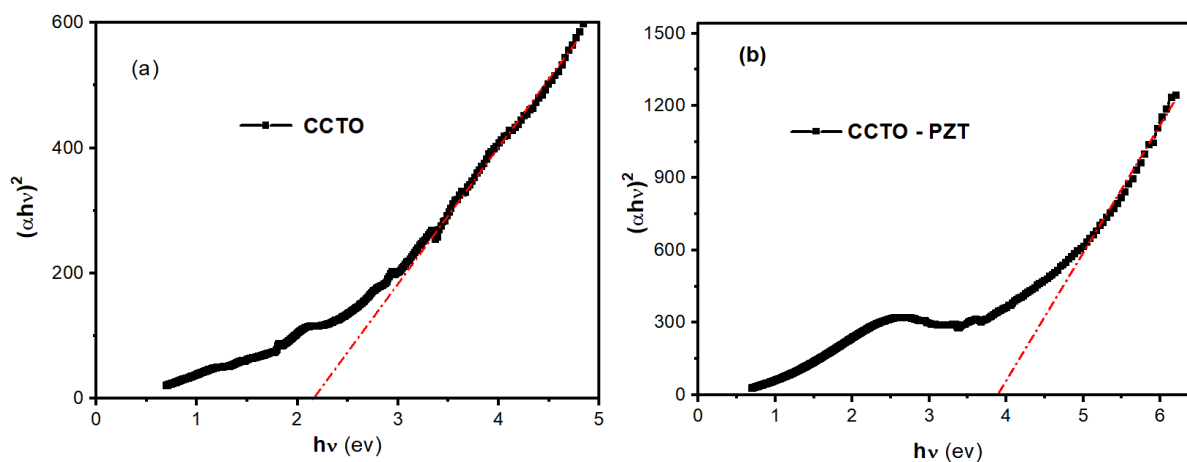

Figure 12. The optical band gap energy of CCTO and CCTO-PZT

Table 3. The optical transmittance and band gap energy of CCTO, CCTO-PZT and PZT composites.

Composite	transmittance	Energy gab (ev)
CCTO	46.43	2.25
CCTO-PZT	69.24	3.92
PZT	99.22	3.50

Conclusion

The present work reports the results of our study on the dielectric and electrical properties of CCTO-PZT composite ceramics. $(1-x)CaCu_3Ti_4O_{12} - xPZT$ samples were synthetized with compositions x = 0.00, 0.50 and 1.00. X-ray diffraction pattern shows pure cubic and tetragonal phase for x = 0.00 and x= 1.00 compositions respectively, while the x = 0.50, composition presents a composite phase cubic and tetragonal. The diffraction peaks in the pattern of the composite sample do not reveal any change in the structures of both CCTO and PZT in the mixture. From Rietveld refinements, the obtained values of the lattice parameters are close to the reported values in the literature. Scanning electron micrographs show a uniform grain distribution and the grain sizes and shapes depending on the PZT amount in the composite. The dielectric measurements show that the CCTO- PZT presents higher values of the dielectric constant. The Curie temperature was found to be 400 ^{o}C for pure PZT, and it is shifted toward a lower temperature ($T_c \sim 340$ ^{o}C) in CCTO-PZT. The electrical property indicates that the material exhibits a single semi circular arc at lower temperatures attributed to grain bulk conduction, and for higher temperatures, the semicircle arc is distorted by the appearance of another arc attributed to the grain boundary conduction. The temperature evolution of the diameters of the arcs suggests that the materials present a negative temperature coefficient resistance (NTCR). A temperature dependent relaxation phenomenon is observed for the CCTO-PZT sample; the ac conductivity increases with increasing the temperature and obey the Arrhenius law. Optical transmittance spectra show that PZT is more transparent than CCTO-PZT and PZT, the optical band gap energies (E_g) were found to be 2.25 eV, 3,51 eV, 3.92 eV for CCTO, PZT and CCTO-PZT respectively.

References

1- U. S. Rai Singh L, K. D. Mandal, N. B. Singh An Overview on Recent Developments in the Synthesis, Characterization and Properties of High Dielectric Constant Calcium Copper Titanate Nano-Particles. Nanosci Technol. **2014**, 1(2) 1-17.

2- A. Deschanvers, B. Raveau, F. Tollemer. Substitution of Copper for a divalent metal in perovskite-type titanates. *Bull. Soc. Chim*. Fr. **1967**, 4077-4078.

3- S. Laxman, U. S. Rai, K. D. Mandal and N. B. Singh. Progress in the growth of $CaCu_3Ti_4O_{12}$ and related functional dielectric perovskites progress in Crystal Growth and Characterization of Materials, **2014**, 60, 15–62, http://dx.doi.org/10.1016/j.pcrysgrow.2014. 04.

4- N. Hadi T. Lamcharfi F. Abdi, A. Elbasset, and S. Sayouri. Effect of Sintering Temperature on the Dielectric and Microstructure Properties of $CaCu_3Ti_{3,90}Co_{0,10}O_{12}$ Ceramic *International Journal of Development Research*, **2017**, 07, (04) 12432-12436.

5- S, Laxman, U. S Rai, K. D, Mandal and A. K Rai. Effect of site selection on dielectric properties of Fe doped $CaCu_3Ti_4O_{12}$ electro-ceramic synthesized by citrate nitrate gel *Indian J Phys,* **2014**, 88 **(7)** 665–670.

6- K. Raju, R. Rashmi and S. Seema Influence of $BiFeO_3$ addition on the electrical properties of $(Na, K) (Nb, Ta)O_3$ ceramic system using impedance spectroscopy *Adv. Mat. Lett*. **2014**, 5(11), 658-665.

7- C. Arun, S, Hemant, U C. Naithani, S. Shubhash, P, D, Pratiksha M. Anuradha, Alok Srivastava, R..K. Sharma. Structural, dielectric and electrical properties of Lead zirconate titanate and $CaCu_3Ti_4O_{12}$ ceramic composite *Adv. Mat. Lett*., **2011**, 2(1), 26-3.

8- S. Laxman, U. S. Rai, K. D. Mandal and A. K. Rai. Effects of partial substitutions of transition metal cations on dielectric properties of $Ca_{1-x}La_xCu_{3-x}Mn_xTi_{4-x}Ni_xO_{12}$ (x= 0.05, 0.10) electro-ceramics synthesized by semi-wet chemical method. Journal of Advanced Ceramics, **2013**, 2, 119–127.

9- A. F. L Almeida, P. B. A. Fechine, V .Góes, M. A. Valente, M. A. R .Miranda and A. S. B. Sombra Dielectric properties of $BaTiO_3$-$CaCu_3Ti_4O_{12}$ composite screen-printed thick films for high dielectric constant devices in the medium frequency (MF) range, Mater. Sci. Eng., **2004**, 111-113.

10- N. Hadi, T, Lamcharfi, F. Abdi, N. Gouitaa, N. S. Echatouiand M. Zouhairi Structural, Dielectric and Electrical Properties of (1-x) $CaCu_3Ti_4O_{12}$-(x) $BaTiO_3$ Ceramics Journal of chemistry: **2017**, vol. 29. No, (8)1811-1816.

11- N. Hadi. T.E. Lamcharfi, F. Abdi, N. S. Echatoui, F Z. Ahjyaje A. Harrach and S. Chouikh, the study of the dielectric, and micro-structure properties of (1-x) $CaCu_3TI_4O_{12} - (x)$ $PbZr_{0.65}Ti0._{35}O_3$ composite, IOP Conf. Series: Earth and Environmental Science, **2018**; 161. https://iopscience.iop.org/article/10.1088/1755-1315/161/1/012020.

12- A. Rajabtabar-Darvishi, W.L. Li, O. Sheikhnejad-Bishe, L.D. Wang, Y. Zhao, S.Q. Zhang, W.D. Fei, Dielectric properties of $CaCu_3Ti_4O_{12}/Pb(Zr_{0.52}Ti_{0.48})O_3$ composite

ceramics Journal of Alloys and Compounds 514, **2012**, 179– 182

13- R. S. Ernest Ravindran, P. Thomas and S. Renganathan, Effect on dielectric, structural and thermal behaviour of CaCu3Ti4O12 in a Nylon 11 matrix, Bull. Mater. Sci., 2019, 42:28 https://doi.org/10.1007/s12034-018-1707-y.

14- R. A. Young, "The Rietveld Method" International Union of Crystallography, New York, Oxford University Press **1996**.

15- M.A Subramanian,.; A.W Sleight,.$ACu_3Ti_4O_{12}$ and $ACu_3Ru_4O_{12}$ perovskites: high dielectric constants and valence degeneracy Solid State Sciences, **2002**, 4, 347-351.

16- J. Frantti, J. Lappalainen, V. Lantto, H. Rundlof, S. Nishio, S. Eriksson, S. Ivanov, M. Kakihana, Neutron diffraction studies of Pb $(Zr_xTi_{1-x})O_3$ ceramics, Japanese Journal of Applied Physics, Part 1, **2000**, 39, 5697-5703.

17- N. Sahu, M. Kar and S. Panigrahi, "Rietveld Analysis of a single phase $PbTiO_3$, Proceedings of NCMSTA"08 Conference November **2008**, 13-14.

18- J. Mohammed, Tchouank Tekou Carol T., H.Y. Hafeez, D. Basandrai, Gopala Ram Bhadu, Sachin Kumar Godara, S.B. Narang, A.K. Srivastava, Electromagnetic interference (EMI) shielding, microwave absorption, and optical sensing properties of BaM/CCTO composites in Ku-band, Results in Physics, **2019**, Vol.13, 102307, doi:10.1016/j.rinp.2019.102307.

19- R. Jenkins and R. L. Snyder "*Introduction to X-ray Powder Diffractometry*",1996, John Wiley & Sons, Inc.

20- M. Sahu · R. N. P. Choudhary, Processing and Electrical Characteristics of Barium Doped CaCu3Ti4O12, Transactions on Electrical and Electronic Materials, **2019**, Volume 20, Issue 1, pp 16–23, https://doi.org/10.1007/s42341-018-0073-1.

21- A. P. Barranco, J. D. L. S. Guerra. Dielectric relaxation related to single-ionized oxygen vacancies in $(Pb_{1-x}La_x)(Z_{0.90}Ti_{0.10})_{1-x/4}O_3$ ceramics, Mater. Res. Bull., **2010**, 45, 1311.

22- M. P. Moret, M. A. C. Devillers, K. Worhoff and P. K. Larsen, Optical properties of $PbTiO_3$, $PbZr_xTi_{1-x}O_3$, and $PbZrO_3$ films deposited by metalorganic chemical vapor on SrTiO3, Journal of Applied Physics, **2002**, 92, 468-474.